Water Air Soil Pollut (2024) 235:692
https://doi.org/10.1007/s11270-024-07503-9

Remediation of Cr(VI)-Contaminated Soil Based on Cr(VI)-Reducing Bacterium Induced Carbonate Precipitation

Chunyangzi Jiang · Liang Hu · Ni He · Yayuan Liu · Hongbo Zhao

Received: 17 April 2024 / Accepted: 7 September 2024

Abstract Microbially induced carbonate precipitation (MICP) provides a novel idea to solve the problem of reduction and stabilization of Cr(VI) in contaminated soil. In this study, the remediation of Cr(VI) in severely polluted soil (total Cr = 5530.00 ± 120.21 mg/kg) by MICP technology combined with the Cr(VI)-reducing bacterium *Sporosarcina saromensis* W5 was systematically investigated. The results indicated that in W5 and $CaCl_2$ treatment after 35 d of remediation, the Cr in exchangeable fraction could be converted into the oxidizable fraction (F3) and the proportion was 41.49%. Compared to original Cr(VI)-contaminated soil, the content of organic matter and soil urease were enhanced after remediation, indicating the improvement of soil quality. The increase in pH also facilitated the formation and stabilization of carbonate precipitation. In addition, the characterization results showed that Cr(VI) in soil was first reduced to Cr(III), and then formed $Ca_{10}Cr_6O_{24}(CO_3)$ coprecipitation with $CaCO_3$. The stabilization mechanism of Cr(VI) contained bioreduction, adsorption/complexation, and coprecipitation. The results of this study proposed an efficient and reliable strategy of Cr(VI)-reducing bacterium combined with MICP technology to reduce and stabilize Cr(VI) in high concentration Cr(VI) contaminated soil.

Keywords Soil remediation · Microbially induced carbonate precipitation · Cr(VI)-reducing bacterium · Bioreduction · Stabilization

1 Introduction

Chromium (Cr), as a commonly observed soil contaminant, has become a major concern worldwide due to the increasingly accumulation in soil (Dou et al., 2022). The two primary states of Cr that are present in contaminated soils, that is, low-mobility trivalent chromium (Cr(III)) and high-mobility hexavalent chromium (Cr(VI)) (Gao et al., 2022). Due to the continuing improper discharge of Cr(VI) waste in industrial processes, causing severe pollution of water and soil, which not only affects plant growth, aquatic organisms and soil environment microecology, but also presents potential risks to human health (Fu et al., 2021; Liu et al., 2023). Trace amounts of Cr(III) have several benefits for the human body, including regulating blood sugar levels, protecting cardiovascular health, and supporting metabolism and energy levels. Nonetheless, the toxicity of Cr(VI)

Supplementary Information The online version contains supplementary material available at https://doi.org/10.1007/s11270-024-07503-9.

C. Jiang · L. Hu (✉) · N. He · Y. Liu · H. Zhao
School of Minerals Processing and Bioengineering, Key Laboratory of Biohydrometallurgy of Ministry of Education, Central South University, Changsha 410083, China
e-mail: huliang2018@csu.edu.cn

Published online: 18 September 2024

is mainly manifested in the oxidative damage to the human body. When the human body ingest excessive Cr(VI), it will produce a large number of reactive oxygen species in the cell, resulting in the damage of cell structure and function. Consequently, there is an urgent need for an eco-friendly remediation strategy to address the soil Cr(VI) pollution. The common method to remediate Cr(VI)-contaminated soil is stabilizing and reducing (Fu et al., 2021). At present, researchers have developed a number of methods for treating Cr(VI)-contaminated soil, such as physical remediation (Wani et al., 2022; Nie et al., 2023), chemical remediation (Li et al., 2022a, 2022b; Tang et al., 2022), microbial remediation (He et al., 2022a, 2022b; Zou et al., 2022).

Because of the eco-friendly and low-cost characteristics, microbial remediation strategy has attracted great attention in recent years (Wu et al., 2022a, 2022b). In particular, a commonly used technique for the remove and immobilize heavy metals in soil is microbially induced carbonate precipitation (MICP) (Song et al., 2022). According to previous studies, ureolytic bacteria hydrolyzed urea by producing urease, releasing NH_4^+ and CO_3^{2-} during MICP process. And then, with the increase of pH, CO_3^{2-} reacted with Ca^{2+} to form insoluble carbonate precipitation such as calcium carbonate ($CaCO_3$) (Qian et al., 2017; Disi et al., 2022; Cai et al., 2023). The effective immobilization of heavy metals in soil by MICP has been demonstrated, which could promote the further adsorption of insoluble carbonate precipitate or form coprecipitation with other heavy metals (Peng et al., 2020). Moreover, studies demonstrate that MICP technology can also enhance the physicochemical properties of soil, mainly because the microorganisms secrete extracellular polymeric substance (EPS) to adsorb carbonate precipitates as well as increase the soil strength, which is conducive to soil improvement (Song et al., 2022; Fu et al., 2023; Kumar et al., 2023). For these reasons, MICP is considered to be a prospective and sustainable method to address the heavy metal pollution.

MICP technology is often used to stabilize heavy metals in soil because calcite is stable in nature (Zeng et al., 2021; Cai et al., 2023; Kumar et al., 2023). In recent years, for example, Sheng et al. (2022) found that Cd(II) could be immobilized in the crystal lattice of calcite by ion exchange with Ca^{2+}, some other studies proved that lots of heavy metals including Pb(II) (Zeng et al., 2021), Zn(II) (Disi et al., 2022), Cr(VI) (Zhang et al., 2022) and Cu(II) (Xue et al., 2022) could also be immobilized to form carbonate precipitates by MICP. In addition, studies indicated that divalent heavy metal ions could be immobilized in soil by replacing the position of Ca^{2+} in the calcite lattice to form precipitates such as $CdCO_3$, $CuCO_3$ and $PbCO_3$ during the MICP process (Song et al., 2022). Although some researches have shown that the trivalent metals such as Cr(III) and As(III) in soil can be effectively fixed in the crystal lattice of calcite or adsorbed on the surface of calcite by MICP (Altowayti et al., 2019; Zhang et al., 2022), it is still unknown how Cr(VI) valence change in soil and its mechanism during MICP process. Cr(III) and Cr(VI) are the two most common stable forms of Cr in soil, and the valence state changes of Cr in soil and its reduction and immobilization mechanism have not been further clarified. At present, the microorganisms used in the MICP research are mostly ureolytic bacteria, however, most of them were difficult to tolerate Cr(VI). In our previous study, the *Sporosarcina saromensis* W5 could not only secrete urease, but also have high Cr(VI) reduction ability and tolerate toxicity (Jiang et al., 2023). Therefore, utilizing alliances between Cr(VI)-reducing bacterium and MICP technology may be a promising solution to effectively reduce and immobilize Cr(VI) in the soil.

In order to accomplish the Cr(VI) reduction and stabilization in the soil, this study used a combination of Cr(VI)-reducing bacterium and MICP technology. This investigation set out to: (1) determine the changes in the chemical speciation of Cr in soil, (2) examine the changes of pH, organic matter (OM) and urease activity during soil remediation, (3) evaluate the valence state of Cr in soil, (4) propose a possible mechanism for using *S. saromensis* W5 and MICP to reduce and immobilize Cr in soil. This study will offer important new understandings of the mechanism by which MICP immobilizes Cr(VI) as well as possible applications for remediating soil contaminated with variable valence heavy metals.

2 Materials and Methods

2.1 Sample Collection and Characteristic Analysis

Top 20 cm of soil samples were collected from Xiangjiang in Changsha, China (28◦ 10′ 3″ N, 112◦ 57′ 1″ E).

The collected soil was spiked with a $K_2Cr_2O_7$ solution and mixed thoroughly, then air-dried for seven days to create an artificially Cr(VI) contaminated soil. The simulated soil was dried and ground then screened with a 100 mesh sieve. Soil pH was determined in Milli-Q water with a 1:2.5 soil-to-solution ratio. The total Cr content was detected by the inductively coupled plasma optical emission spectroscopy (ICP-OES, PerkinElmer Avio500) after triacid digestion (HNO_3–HF–$HClO_4$). The total Cr(VI) in the soil was extracted by the alkaline digestion method and analyzed using the 1,5-diphenyl carbazide method on UV-1780 ultraviolet spectrophotometer (Shimadzu, Japan) at 540 nm (Shi et al., 2020). Soil samples had the following primary physicochemical characteristics: pH = 6.73; organic matter (OM) = 10.78 g/kg; total Cr = 5530.00 ± 120.21 mg/kg; total Cr(VI) = 4574.75 ± 136.76 mg/kg.

2.2 Bacterial Cultivation and Reagents

The Cr-reducing bacterium, *S. saromensis* W5 used in this study was isolated from an abandoned chromite plant in Changsha, Hunan Province, China (He et al., 2014). In the bacterial cultivation experiment, the culture medium consisted of 10.0 g/L peptone, 5.0 g/L yeast extract, 5.0 g/L NaCl, 0.2 g/L $MgSO_4{\cdot}7H_2O$ and 0.05 g/L K_2HPO_4, and the pH was adjusted to 10.0. *S. saromensis* was cultivated in the constant temperature shaker at 30 ℃ and 180 rpm for 12 h. All chemical reagents used in this work were analytical grade reagents.

2.3 Soil Remediation Experiments

A centrifuge tube containing 0.5 g soil sample and 5 mL culture solution was used for five comparative experiments: (1) Biotic control, free *S. saromensis* W5 solution (C_1); (2) & (3) Abiotic controls, (2) free 0.05 g $CaCl_2$ and 0.01 g urea (C_2), (3) free 0.1 g $CaCl_2$ and 0.01 g urea (C_3); (4) & (5) Experimental groups, (4) W5 bacterial solution containing 0.05 g $CaCl_2$ and 0.01 g urea (E_1), (5) W5 bacterial solution containing 0.1 g $CaCl_2$ and 0.01 g urea (E_2). In the treatment group requiring the addition of microorganisms, the volume of the bacterial solution was 100 µL and the concentration of the bacterial solution was 1×10^8 CFU/mL. Each treatment was cultured at 25 ℃ for 1, 7, 14, 21, 28, 35 days. To separate the supernatant and soil, the treated samples were centrifuged at 6000 rpm for 15 min in a centrifuge, and the separated samples were stored at 4 °C for subsequent tests. Three parallel samples were set up in all experiments. The supernatant was used to determine pH, and the soil was used to determine organic matter, urease activity, the content of Cr(VI) and speciation analysis of heavy metals in soil. Additionally, ultraviolet absorption spectrometry was used to detected the Cr(VI) change in the treatment system.

2.3.1 Organic Matter (OM) and Soil Urease Activity

The organic matter (OM) was measured by using the potassium dichromate volumetric dilution heating method (Nelson & Sommers, 1974). To demonstrate how soil urease activity is impacted by Ca^{2+} and urea concentrations, two experimental groups were added on the basis of Section 3: (1) free 0.05 g $CaCl_2$ and 0.02 g urea (C_4), (2) W5 bacterial solution containing 0.05 g $CaCl_2$ and 0.02 g urea (E_3). Urease activity in soil was measured in sodium phenolate-hypochlorite salts methods on a UV–vis spectrophotometer, and the urease activity could be expressed as mg NH_4^+-N produced by hydrolysis per g of soil within 24 h (mg NH_4^+-N/g soil 24 h) (Wei et al., 2022). Specifically, 0.5 g soil was incubated at 37 ℃ for 24 h in a test tube containing 100 µL of toluene, 1 mL of 10% urea solution and 2 mL of citrate buffer (pH = 6.7). The mixture was centrifuged to obtain a supernatant and determined by spectrophotometry at 578 nm.

2.3.2 BCR Sequential Extraction

BCR sequential extraction (European Community Bureau of Reference) was used to determine the fractionation of Cr in soil (He et al., 2022a, 2022b). In brief, 0.11 mol/L HAc was added to extract the exchangeable fraction (F1). The reducible fraction (F2) was obtained by mixing 0.5 mol/L $NH_2OH{\bullet}HCl$ (pH = 2.0) with the solid residue. Next, 30% H_2O_2 was used to oxidize the solid residue and NH_4OAc was added to obtain the oxidizable fraction (F3). And after digesting the residual with HNO_3-HF-$HClO_4$ mixture, the residual fraction (F4) was extracted. The ICP-OES was used to analyze the Cr content in the extractants.

2.3.3 The Ultraviolet Absorption Spectrum of Cr(VI)

Changes of Cr(VI) within the supernatant in different treatment groups after 1 d and 35 d of soil

remediation were detected by ultraviolet spectrophotometer (U-4100, Japan), and the detection wavelength was 250—500 nm (Carter et al., 2012). Deionized water was utilized as the background correction in the control check rather than the culture medium.

2.3.4 Characterizations of the remediated soil

For further understand the properties of the treated soil, it was vacuum freeze-dried for 12 h. The changes of soil surface morphology before and after restoration were analyzed by using Scanning electron microscopy (SEM, JEOL, JSM-7900 F, Japan). After that, freeze-dried precipitated samples were ground into powder for subsequent experiments. Fourier transform infrared spectroscopy (FTIR, WQF-410, China) was used to identify the functional groups. The composition of soil crystal structure was examined by X-ray diffraction (XRD, D8-Advance, Bruker Company, Germany). The valence bond changes of elements after soil restoration were detected by X-ray photoelectron spectroscopy (XPS, Thermo Scientific K-Alpha, America).

3 Results and Discussion

3.1 Cr Fractions in Soil

Depending on their chemical forms, there is a decrease in the heavy metals biotoxicity of soil as stability increased (Wei et al., 2022; Xiao et al., 2023; Xie et al., 2023). Figure 1 illustrated the changes of Cr fractions in soil before and after different treatments. Cr species in CK consisted of four fractions, included exchangeable fraction (F1, 88.69%), reducible fraction (F2, 3.75%), oxidizable fraction (F3, 6.50%) and residual fraction (F4, 1.06%). The proportion of F1 decreased gradually with the increase of remediation time, while the F2 and F3 increased. Compared with the CK group, the F1 fraction of Cr after 35 d of remediation decreased to 14.65% (C_1), 40.03% (C_2), 51.18% (C_3), 19.30% (E_1) and 27.98% (E_2), respectively. On the contrary, the speciation of F3 in treated samples increased to 38.23% (C_1), 31.55% (C_2), 28.18% (C_3), 41.49% (E_1) and 36.36% (E_2), respectively. The results of chemical speciation showed that a proportion of F1 was transformed into F2 and F3. During the 35 d of remediation, the obviously lower proportion of F1 in C_1 was explained by the effective reduction of Cr(VI) by W5 strain. Besides, E_1 showed the most increased proportion of F3 forms, indicating that the Cr(VI) mobility and bioavailability were decreased by the bioremediation of MICP. Moreover, the morphological transformation of E_1/E_2 was more obvious than that of C_2/C_3 because of the significant role of W5 strain in the MICP process. Meanwhile, W5 strain facilitated the transformation of F1 to F2 form. In fact, the study showed that Cr(III) could be further immobilized by combining with functional groups of microbial cells, which were also stable nucleation sites for mineral formation (Fu et al., 2021). Moreover, the conversion ratio of F1 forms in C_3/E_2 were higher than those in C_2/E_1, which corresponded to the concentration of Ca^{2+}. Previous study pointed out that Ca^{2+} addition could facilitate microorganisms growth, alleviate Cr(VI) toxicity as well as promote the Cr(VI) reduction and stabilization (Zhang et al., 2022). Nevertheless, an excessively high concentration of Ca^{2+} would hinder the transformation of Cr fractions by inhibiting urease activity and microbial growth (Zeng et al., 2021).

3.2 The Changes in pH and Organic Matter (OM)

In addition to influencing microbial communities and soil properties, soil pH also had an impact on microbial growth and activity, heavy metal availability and forms (Liu et al., 2023). On 1 d, due to the addition of alkaline medium, the pH ranged from 8.16 to 8.48 in all treatment groups and was obviously higher than in original soil (Fig. 2(a)). In the subsequent 35 d treatment, the pH in C_1 group was the highest at about 9.63. The pH value of the other treatment groups varied from 7.73 to 8.80 compared to the original soil (pH = 6.73). On the one hand, urea hydrolysis produced CO_3^{2-} and NH_4^+ during MICP process, which led to an increase in pH (Peng et al., 2020). From another point of view, the bacteria would produce alkaline metabolites when the culture time was extended, while nucleic acid substances and proteins leaked out, then entered into the incubation system as a result of bacterial autolysis at a later stage, which could also lead to an increase in pH (Zheng & Qian, 2020). Li et al., (2022a, 2022b) found that the pH increased significantly to 8.50 after 28 days of remediation, during the MICP process of immobilizing cadmium by the strain *Bacillus sp*. Furthermore, the

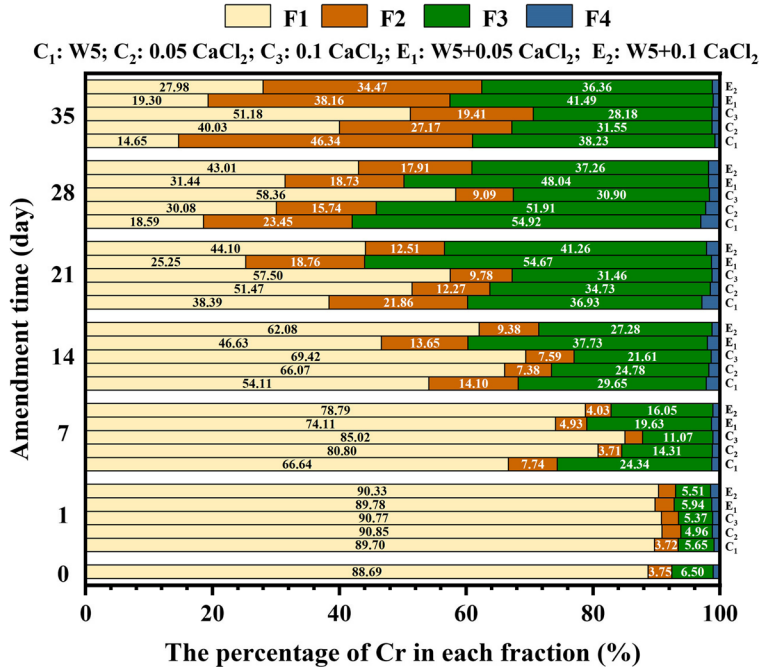

Fig. 1 The distribution of Cr fractions in the treated samples (C_1, C_2, C_3, E_1 and E_2) during 35 d of remediation. Day 0 represents the original data of the untreated sample

studies suggested that $CaCO_3$ precipitation was more stable under alkaline conditions (Song et al., 2022; Xue et al., 2022; Fu et al., 2023). Moreover, a high pH also promoted the form transformation of Cr(VI) (Zhang et al., 2023), which was coincided with the results of chemical speciation from BCR showed that a proportion of F1 was transformed into F2 and F3 during the 35 d of remediation.

The organic matter is an important index for evaluating soil fertility, which have an impact on both the Cr chemical form and microbial growth (Wani et al., 2022). As shown in Fig. 2(b), OM in each group increased obviously on 1 d, which might be due to the addition of medium. On 35 d, the OM content of soil in each treatment groups increased significantly with the following sequence: $E_2 > C_3 > E_1 > C_2 > C_1$. For one thing, the addition of urea and $CaCl_2$ would enhance the growth and activity of native microorganisms. And for another, compared with the native microorganisms, W5 could more efficiently participate in reducing and immobilizing of Cr(VI) in soil and reduce its bioavailability, which would also increase the tolerance of soil microorganisms to Cr(VI) and thus enhance the microbial bioactivities. The increase in soil organic matter content could be explained by the growth and multiplication of native microorganisms and strain W5 by utilizing nutrients in the addition medium, which also produced new organic matter in the process (Dong et al., 2022). Therefore, the interaction among urea and $CaCl_2$, heavy metals and microorganisms should be cause of the change in OM content. Additionally, the Cr(VI) reduction and stabilization was facilitated by the abundant carboxyl, hydroxyl, amine and other active groups in OM (Gao et al., 2022). It was also found that OM was not only an electron donor in Cr(VI) reduction, but also be a major ligand for complexing with Cr in soil (Lin et al., 2019).

3.3 The Total Cr(VI) Content in Soil

Cr(III) have less toxicity and migration in soil than Cr(VI), which can be stabilized by adsorption, precipitation or reduced to Cr(III) (Shi et al., 2020). Cr(VI) and reduced Cr(III) in soil may be adsorbed to the surface of soil particles, or form stable forms including carbonate or hydroxide (Tang et al., 2022). Figure 3(a) illustrated the influence of various treatments in total Cr(VI) reduction in soil. On 1 d, chromium was mainly present as Cr(VI). The Cr(VI) content in each treatment group gradually decreased as remediation time increased, which indicated a reduced risk of Cr (VI) contamination and toxicity after remediation. The residual Cr(VI) content in C_1, C_2, C_3,

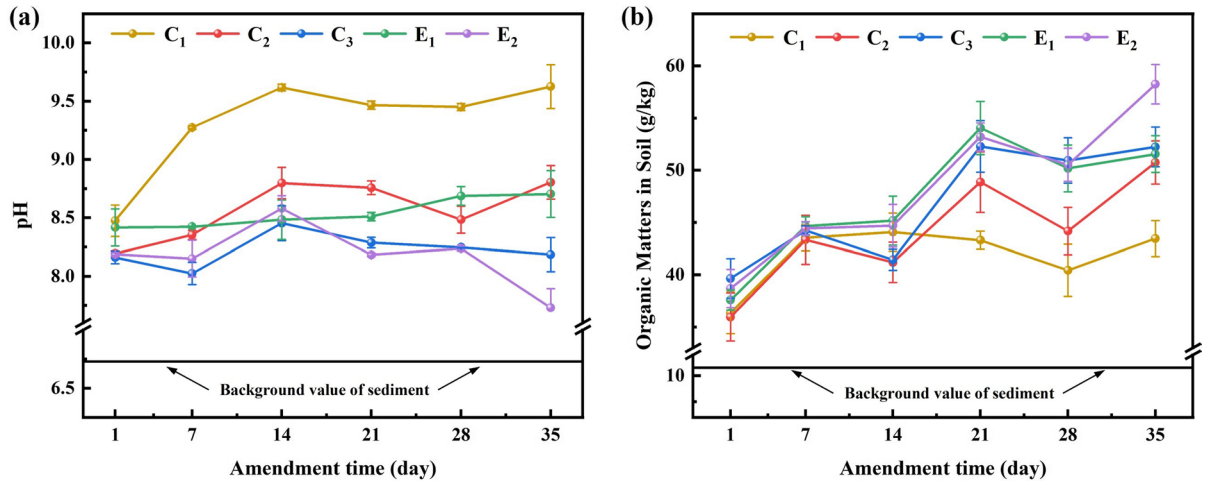

Fig. 2 The change of pH (**a**) and organic matters (**b**) in different treated samples during 35 d of remediation. C_1, C_2, C_3, E_1 and E_2 represent W5, 0.05 g $CaCl_2$, 0.1 g $CaCl_2$, W5 + 0.05 g $CaCl_2$ and W5 + 0.1 g $CaCl_2$ treated samples, respectively. The error bars represent the standard deviation of the means ($n = 3$)

E_1 and E_2 samples were 8.29 mg/kg, 331.77 mg/kg, 2378.97 mg/kg, 5.75 mg/kg and 38.57 mg/kg, respectively, after 35 d of remediation. The form changes of total Cr in the system were depicted in Fig. 3(b). On 14 d of remediation, the reduction rate of Cr(VI) in C_1 and E_1 reached 99.40% and 99.57%, respectively, and kept constant. The Cr(VI) reduction rate in E_2 was 97.88% on 28 d. Microorganisms could reduce Cr(VI) through two pathways: one is to produce reductase to directly reduce; the other is to reduce Cr(VI) through some reducing metabolites of microorganisms, such as EPS (Zhang et al., 2014; Luo et al., 2022; Ma et al., 2022). After 35 d of remediation, the reduction rates of C_1, E_1 and E_2 were significantly higher than those of C_2 and C_3, which could be explained by the fact that, in comparison to the native microorganism, the W5 strain had a stronger Cr(VI) reduction ability. Additionally, the reduction rate of C_2/E_1 was higher than those of C_3/E_2 at the same time period, which suggested that the addition of an appropriate amount of Ca^{2+} might promote reduction of Cr(VI). Simultaneously, Ca^{2+} also provided mineralization sites for Cr biomineralization. However, excessive Ca^{2+} would inhibit the Cr(VI) reduction (Zhao et al., 2021). As a result of the liquid medium added to the soil system during remediation, there might be a phenomenon that the migration of free Cr(VI) from soil into supernatant. Therefore, the changes of chromium content in soil and supernatant were specifically described in Fig. 3(c) and Fig. 3(d), respectively. According to the results, a major portion of the free Cr(VI) was transferred into the supernatant on 1 d. The Cr(VI) content in soil was decreased in all groups after 35 d of remediation, especially in C_1 and E_1 treatment groups, whose remaining Cr(VI) content were 5.46 and 15.12 mg/kg, respectively. The similar phenomenon also existed in the supernatant system. The remaining Cr(VI) content in C_1, C_2, C_3, E_1 and E_2 treatment groups were 2.83 mg/kg, 103.40 mg/kg, 2410.02 mg/kg, 1.66 mg/kg and 5.08 mg/kg, respectively. To summarize, Cr(VI) both in soil and supernatant would be converted to Cr(III) with low toxicity.

3.4 The Changes of Cr(VI) in the Supernatant

For detecting whether the free Cr(VI) in soil was transferred to the supernatant then immobilized by MICP reaction, the changes of ultraviolet absorption spectra of the supernatant in different treatment groups on 1 d and 35 d were measured (Fig. 4). According to the intensity of absorption peak, it could be judged that the absorption peak of Cr(VI) was at 350—400 nm (Jiang et al., 2023), and the absorption peak at 300—350 nm was dissolved organic matter (DOM) in the soil (Carter et al., 2012). The aromatic or unsaturated compounds and their double bonds (C = C, C = O and N = N)

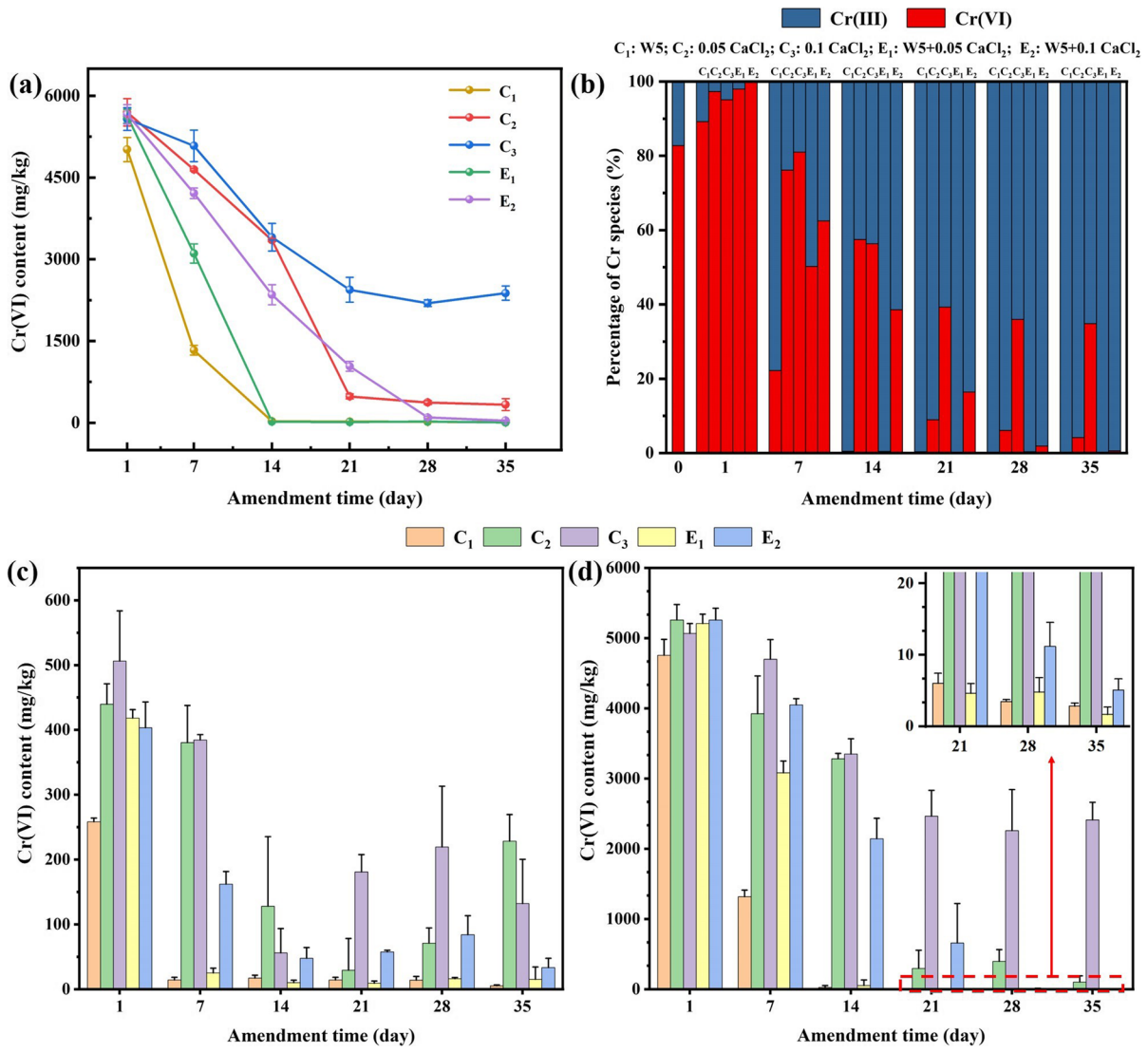

Fig. 3 Changes in the total Cr(VI) content (**a**), the form of Cr (**b**), the Cr(VI) content in soil (**c**) and the Cr(VI) content in supernatant (**d**) with different treatments during 35 d of remediation. The error bars represent the standard deviation of the means ($n = 3$)

in DOM were found in the range of 250—300 nm. Because of the existence of heavy metal ions, Cr would combine with DOM thus shifting its UV absorption peaks (Xie et al., 2021). The reason for more and disorderly absorption peaks might be that the soil system was complex and the organic matter content was high, which might interfere with the absorption peaks. The absorption peaks of C_1 group changed obviously, while those of the abiotic control groups (C_2 and C_3) changed little, suggesting that W5 was mainly involved in Cr(VI) reduction. The absorption peaks of supernatant (refer to Cr(VI) content) at 350—400 nm gradually shifted to the left after 35 d of remediation, indicating that W5 was mainly involved in Cr(VI) reduction and the active Cr(VI) was gradually decreased. Moreover, the absorption peak of the combined treatment group with W5 and $CaCl_2$ (E_1, E_2, E_3) showed the largest change, which indicated that Ca^{2+} supplementation might lessen the Cr(VI) toxicity and thus promote Cr(VI) reduction (Luo et al., 2020). Combined with the previous result of Cr(VI) content in

supernatant, there were fewer ultraviolet absorption peaks at 350—400 nm because of the lower content of residual Cr(VI).

3.5 Changes in Soil Urease Activity

The organic matter content, microbial growth, and soil physicochemical characteristics were all strongly correlated with soil urease activity (Wei et al., 2022), as well as affected the efficiency of MICP (Cai et al., 2023). Urease was able to hydrolyze urea to produce CO_3^{2-} and NH_4^+, and the pH in the system increased, this was a key step in MICP process. The urease activity of original soil was 0.038 mg NH_4^+-N/g soil 24 h (dashed line in the figure), as presented in Fig. 5. When compared to the original soil, the urease activity of all treatment groups was lower on 1 d. One reason was that urease could be poisoned by Cr(VI). In addition, the added culture medium, $CaCl_2$ and urea had not been fully utilized by microorganisms, resulting in the slow growth of microorganisms, which then affected the urease production. After 35 d of remediation, it was found that the urease activity of all groups displayed an increasing trend with the following order: W5 (C_1, 0.757) > W5 + 0.05 $CaCl_2$ + 0.01 Urea (E_1, 0.650) > W5 + 0.1 $CaCl_2$ + 0.01 Urea (E_2, 0.538) > 0.05 $CaCl_2$ + 0.01 Urea (C_2, 0.473) > 0.05 $CaCl_2$ + 0.02 Urea (C_4, 0.429) > 0.1 $CaCl_2$ + 0.01 Urea (C_3, 0.428) > W5 + 0.05 $CaCl_2$ + 0.02 Urea (E_3, 0.252). The treatment group with W5 (C_1) had the highest urease activity, which might be due to the absence of substrate in the culture system so that urease consumed less and remained active. The results indicated that adding ureolytic bacteria could increase soil urease activity (Peng et al., 2020). Besides, the urease activity decreased as $CaCl_2$ dosage increased, suggesting that the appropriate concentration of Ca^{2+} could promote microbial growth and urease secretion, but a high Ca^{2+} concentration suppressed bacterial activity (Sheng et al., 2022). Likewise, the similar result was observed in treatment groups with different urea concentrations, illustrating that too high urea concentration would also inhibit the secretion of urease by bacteria. In conclusion, all treatment groups favored an increase in urease activity compared to the original soil, with the W5 treatment group (C_1) presenting the highest urease activity.

3.6 Characterizations of the Contaminated Soil

3.6.1 Scanning Electron Microscope (SEM)

In Fig. 6, the microscopic morphologies of different treated soil were observed using SEM. The Cr(VI)-contaminated soil was comprised of irregular lumps (Fig. 6(a)), in which EDS spectra showed elements of C, O, Si and Cr (Fig. S1(a)), suggesting that these particles could be organic substances or soil minerals like silicates (He et al., 2022a, 2022b). The surface of the soil sample treated with W5 bacteria became rough as presented in Fig. 6(b), indicating that the microorganisms and their secretions adhered to the surface of the soil particle, which implied that large soil particles could serve as places where microorganisms could attach themselves (Long et al., 2023). In addition, the elemental composition of the W5 treated sample did not significantly differ from the untreated soil sample (Fig. S1(b)). Figure 6(c) showed that the soil formed agglomerates with many particles attached to the surface after treatment with $CaCl_2$. Combined with the increase of Ca and Cr element content in EDS results (Fig. S1(c)), it was speculated that carbonate and Cr formed co-precipitation. In the W5 and $CaCl_2$ treatment, it could be clearly seen that the soil aggregate became larger and presented a square structure (Fig. 6(d)), which was inferred to be calcite structure according to EDS (Fig. S1(d)). According to the previous research, it showed that the precipitation of Cr and carbonate could be combined with soil particles (Song et al., 2022). Meanwhile, it could be observed that the surface of the agglomerates is rough with many particles attached, which might be metabolites of microorganisms and adsorption or co-precipitation of Cr (Peng et al., 2020). In addition, combined with EDS map spectrum in Fig. S2, it could be further demonstrated that Cr and Ca form a co-precipitation.

3.6.2 Fourier Transform Infrared Spectroscopy (FTIR)

FTIR was used to analyzed the changes in functional groups of different treated soil samples (Fig. 7). The stretching vibrations of -OH

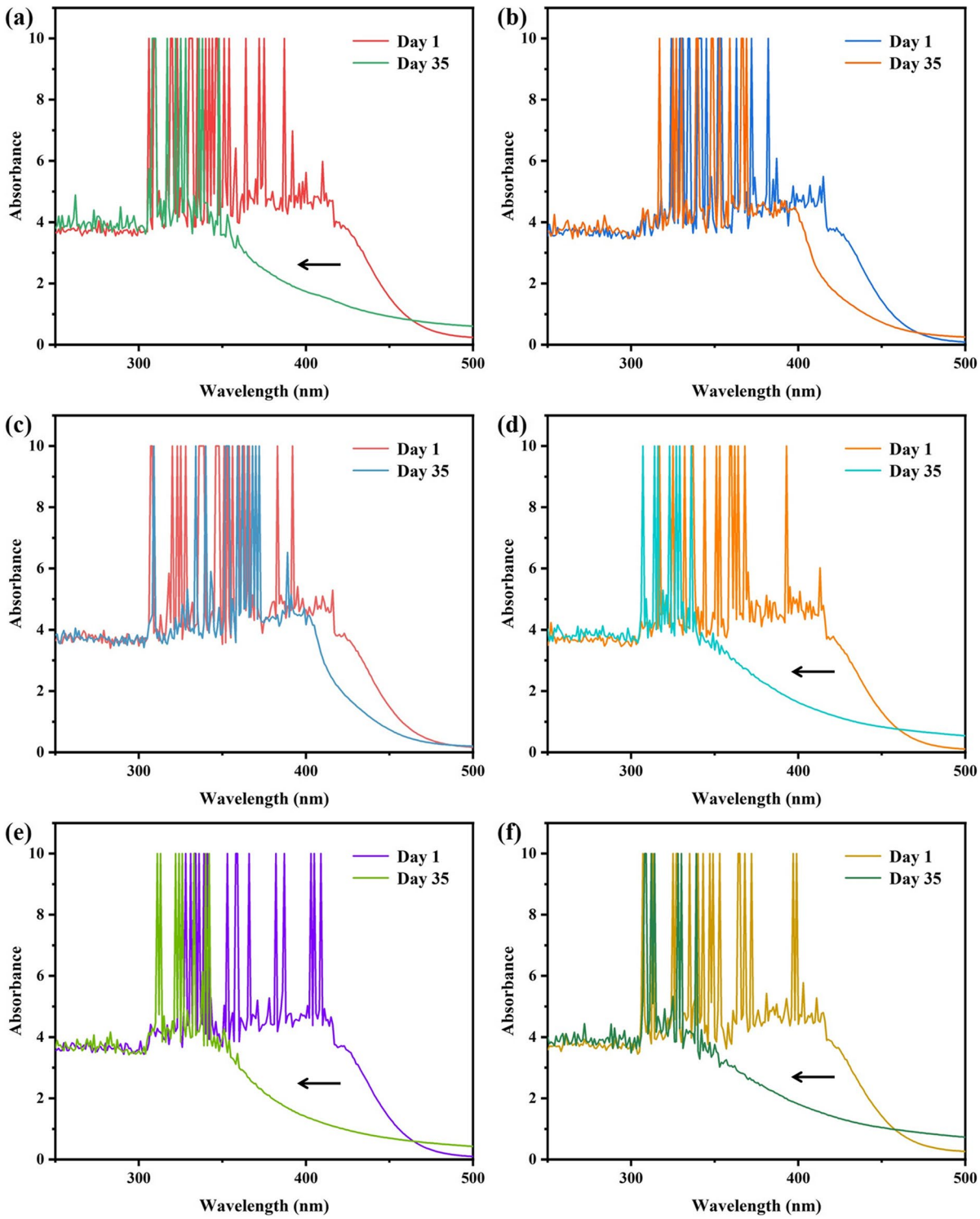

Fig. 4 The UV absorption spectra of supernatant after 1 d and 35 d of remediation with different treatments: (**a**) C_1; (**b**) C_2; (**c**) C_3; (**d**) E_1; (**e**) E_2; (**f**) E_3

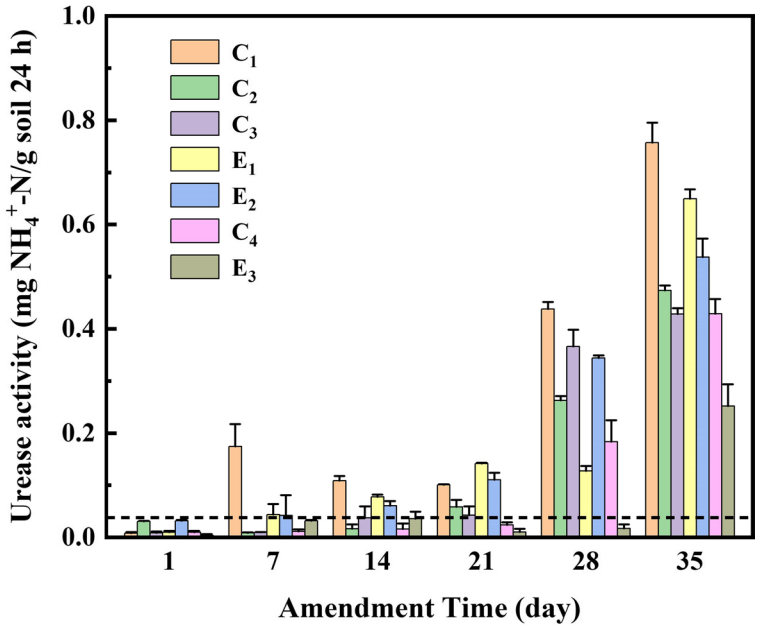

Fig. 5 Changes in the soil urease activity in different treatments during 35 d of remediation. Dashed line represented the urease activity of original Cr(VI)-contaminated soil. The error bars represent the standard deviation of the means ($n = 3$)

group were appeared at 3699 cm^{-1}, 3624 cm^{-1}, 3620 cm^{-1}, 3622 cm^{-1} and 3626 cm^{-1} (He et al., 2022a, 2022b). Besides, the C = O/C = C stretching was found to be the cause of the peak at 1651 cm^{-1} (He et al., 2022a, 2022b; Li et al., 2023). After different treatments, the C = O symmetric stretching vibrations in $v(CO_3^{2-})$ group at 1415 cm^{-1}, 1413 cm^{-1}, 1411 cm^{-1} and 1409 cm^{-1} appeared, in comparison with the original soil (Zeng et al., 2023), which revealed that carbonate precipitation was generated during the MICP reaction. In comparison, the absorption peaks of the W5 strain and the Ca^{2+} treatment groups were more obvious, illustrating that their combination could generate more carbonate to participate in the immobilization of Cr. Additionally, the stretching vibrations of C-O resulted in peaks at 1016 cm^{-1}, 1041 cm^{-1}, 1029 cm^{-1}, 1026 cm^{-1} and 1018 cm^{-1} (Ma et al., 2022), and the characteristic peaks shifted and the intensity increased slightly, demonstrating that C-O was involved in the reaction. The vibration of the Cr–O bond was explained by the peaks observed at 912 cm^{-1} and 796 cm^{-1} in both the original and treated soil samples (Qian et al., 2017). The absorption peak intensity of each treatment group was different, which proved the cooperative interaction with biological reduction and carbonate precipitation for removing Cr from soil. Furthermore, the peak found at 694 cm^{-1} was also identified as C = O vibration of carbonate $v(CO_3^{2-})$ in calcite crystals (Li et al., 2022a, 2022b). The stretching vibration of the bending vibration of Si–O in soil mainly appeared at 543 cm^{-1}, 534 cm^{-1}, 549 cm^{-1}, 538 cm^{-1}, 540 cm^{-1} and 547 cm^{-1} (He et al., 2022a, 2022b). To sum up, -OH, C = O, C-O and carbonate groups were thought to be participated in the soil remediation process.

3.6.3 X-ray Diffraction (XRD)

The component variations in the original soil and different treated samples were described by using XRD. As the result shown in Fig. S3, SiO_2 was the main component in the Cr(VI)-contaminated soil, and $CaCO_3$ also existed. And in the sample treated with W5, the main components in soil were basically unchanged. Compared to the Cr(VI)-contaminated soil, $CaCO_3$ and $Ca_{10}Cr_6O_{24}(CO_3)$ appeared to be the dominant mineral component in the soil in the $CaCl_2$ added treatment groups, while other potential precipitates including $Cr(OH)_3$, Cr_2O_3 and Cr complexed compounds might not be detected (Dou et al., 2022). The reason might be that the soil system was complex and the final product accounted for a small percentage, which was difficult to detect (Fu et al., 2021). However, the SiO_2 peak showed lower intensity in

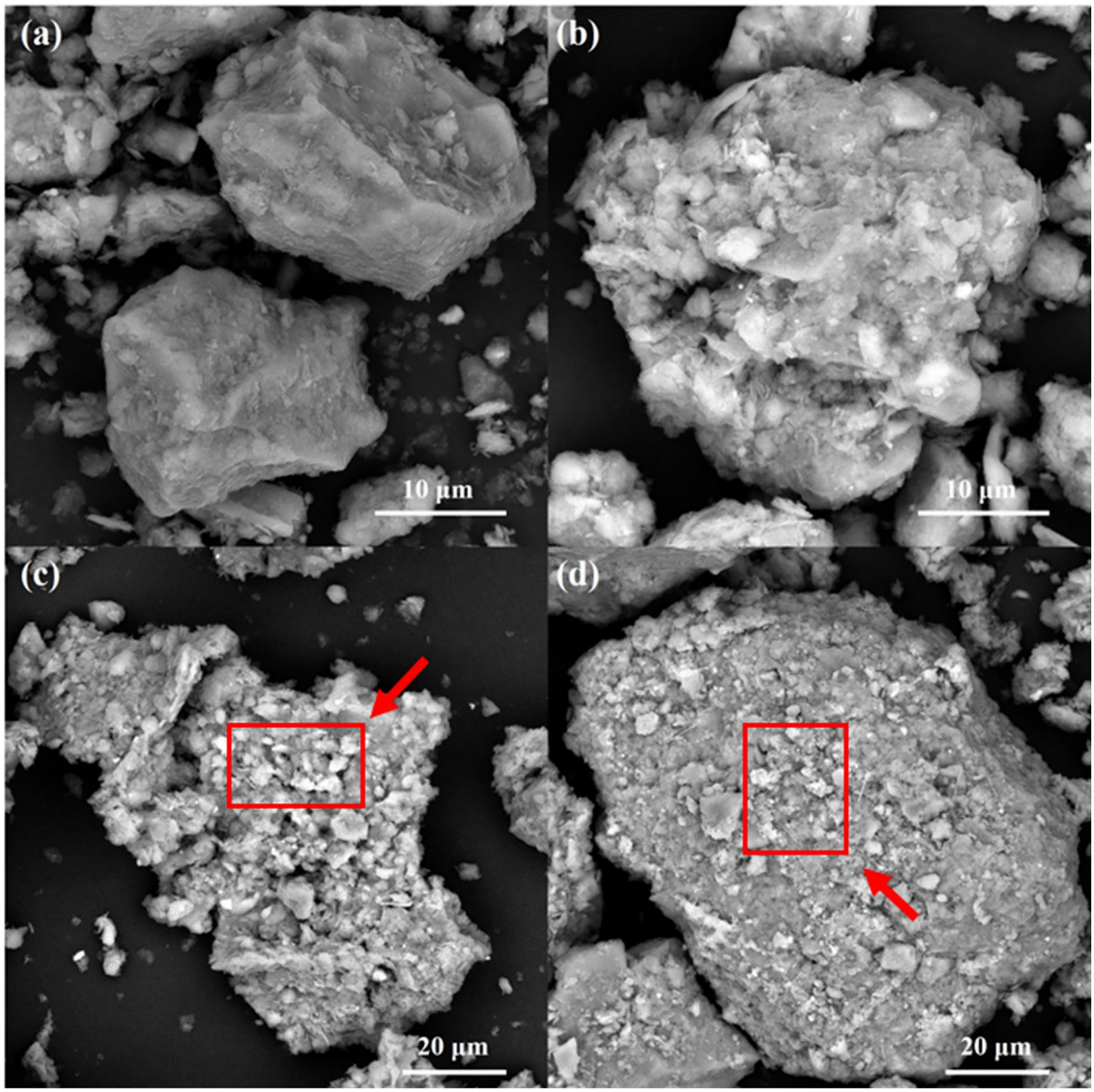

Fig. 6 SEM of soils after remediation with different treatments: (**a**) Cr(VI)-contaminated soil, × 5000; (**b**) soil treated with W5, × 5000; (**c**) soil treated with $CaCl_2$, × 2000; (**d**) soil treated with W5 and $CaCl_2$, × 2000

these four groups of samples, which might be due to some elements being available to microorganisms or adsorbed on the microbial surfaces (Wu et al., 2022a, 2022b). Besides, in the 0.1 $CaCl_2$ treatment group, the peaks of precipitates were more obvious than other treatment groups, which demonstrated that the high Ca^{2+} concentration facilitated the formation of stable crystal forms of Cr during MICP process.

3.6.4 X-ray Photoelectron Spectroscopy (XPS)

The primary chemical components of the soil both before and after remediation were further examined using XPS, which also helped to reveal the mechanism of Cr(VI) reduction and immobilization. The peaks at 284.70 eV, 288.30 eV, 293.20 eV and 295.90 eV belonged to C = C (59.66%), C = O

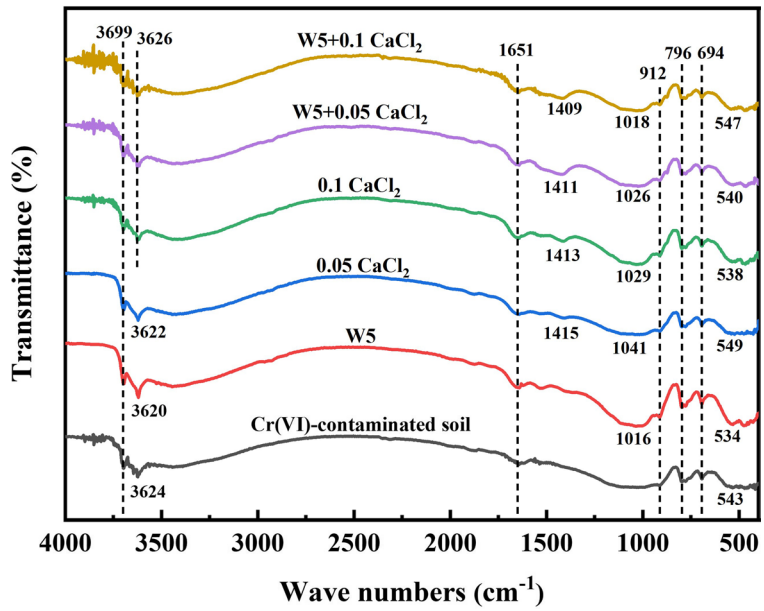

Fig. 7 The FTIR spectra (400—4000 cm^{-1}) of the Cr(VI)-contaminated soil and different treatment soil samples. The black line represents original Cr(VI)-contaminated soil, and the red, blue, green, purple and yellow lines represent W5, 0.05 g $CaCl_2$, 0.1 g $CaCl_2$, W5 + 0.05 g $CaCl_2$ and W5 + 0.1 g $CaCl_2$ treated Cr(VI)-contaminated soil, respectively

(8.09%), C-O (22.14%) and C-H (10.11%) as shown in the C 1 s XPS spectra (Fig. 8(a)) (He et al., 2023; Y. Li et al., 2022a, 2022b). After soil remediation by W5 and $CaCl_2$, the peaks of C = O shifted to 287.82 eV and the peak area increased to 25.22%, simultaneously, the area of C = C also increased to 63.42%, while the areas of C-O and C-H decreased to 5.64% and 5.73%, respectively, which proved that carbonates were formed in the MICP process. Three peaks, measuring 530.99 eV, 531.67 eV, and 532.34 eV, as shown in Fig. 8(b), were attributed to -OH, C = O and O-C = O and were identified in the O 1 s spectrum (Munir et al., 2020; Jiang et al., 2023), respectively. Although there was no significant change in binding energy, the remediation reaction resulted in decreasing the O-C = O intensity ratio from 42.84% to 25.49% and increasing the area of C = O bonds from 21.82% to 41.99%, which was thought to be caused by urease secreted by microbes breaking down urea to produce CO_3^{2-}, further formed carbonate co-precipitation with Ca^{2+} and Cr (Li et al., 2019; Cai et al., 2023). The findings were consistent with the final product in XRD spectrum and the vibrations of C = O in $\nu(CO_3^{2-})$ group in FTIR spectrum. In addition, the Ca 2p spectrum consisted of two peaks at 347.00 eV (Ca $2p_{3/2}$) and 350.90 eV (Ca $2p_{1/2}$) (He et al., 2022a, 2022b) as presented in Fig. 8c, with the area ratios of 44.65% and 55.35%, respectively. After the soil remediation, the peaks of Ca $2p_{3/2}$ and Ca $2p_{1/2}$ not only shifted to 347.10 eV and 350.60 eV, but the area of Ca $2p_{3/2}$ also improved to 64.26%, meanwhile, that of Ca $2p_{1/2}$ decreased to 35.74%. These changes further demonstrated that Ca^{2+} could form $CaCO_3$ precipitate or a coprecipitation with chromium, $Ca_{10}Cr_6O_{24}(CO_3)$. The Cr 2p spectrum broke down into two characteristic peaks at 578.61 eV (Cr $2p_{3/2}$) and 586.47 eV (Cr $2p_{1/2}$) before remediation, which were attributed to Cr(VI) and Cr(III), respectively, as Fig. 8(d) depicted (Wen et al., 2022). As a result of the reaction, the peak of Cr $2p_{3/2}$ was found a shift to 577.10 eV and indicated that Cr(III) was existed. Besides, a notable increase in the Cr(III) area was observed, which accounted for all valence states. A portion of Cr(III) could form many Cr(III) by-products including $Cr(OH)_3$, Cr_2O_3, $CrCl_3$ as well as organic Cr(III) complexes, besides the main formation of carbonate precipitation, according to previous researches (Huang et al., 2021a, 2021b; Dou et al., 2022; Zou et al., 2022). These results confirmed that Cr(VI) was formed into Cr(III) through reductive reaction during the soil remediation. To conclude, the functional groups C = O, C-O, C–C and O-C = O were essential to the Cr(VI) reduction and immobilization process. Moreover, microorganisms

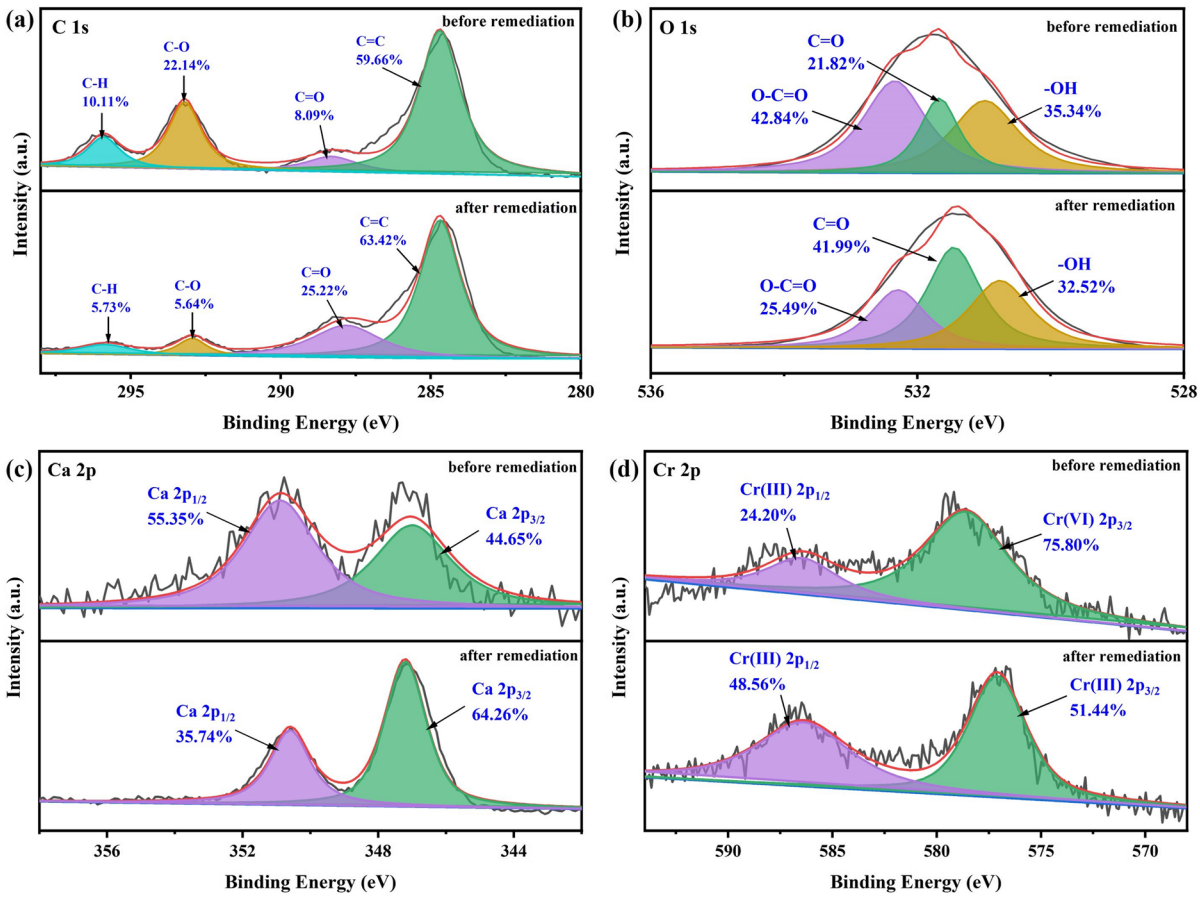

Fig. 8 XPS spectra of (**a**) C 1 s; (**b**) O 1 s; (**c**) Ca 2p; (**d**) Cr 2p before and after remediation in soil

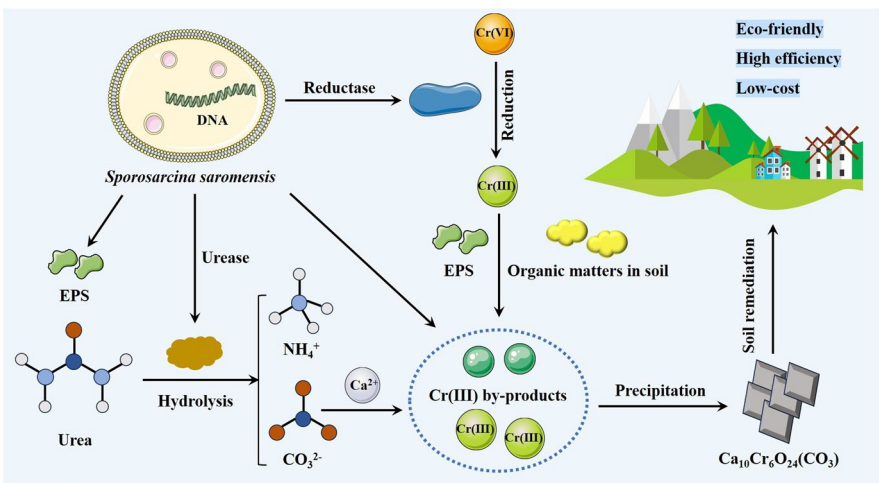

Fig. 9 Proposed remediation mechanism of Cr(VI)-contaminated soil by *S. saromensis* W5 and MICP technology

could reduce Cr(VI) to lower toxic or non-toxic Cr(III) compounds, and further form coprecipitation with calcium carbonate in the MICP process, thus completing the remediation of Cr(VI)-contaminated soil.

3.7 Potential Mechanism for Remediating Cr(VI)-Contaminated Soil

In accordance with the above analysis, Fig. 9 provided a more detailed description of the mechanism for Cr remediation in polluted soil through using Cr(VI)-reducing bacterium *S. saromensis* W5 in combination with MICP technology, which could be mainly divided into the following three steps. Firstly, *S. saromensis* W5 produced reductase and some EPS, which could not only participate in the reaction of reducing Cr(VI), which is highly bioavailable in soil, to less bioavailable Cr(III), but also contribute to the soil fertility improvement through an enhancement of soil organic matter content. Secondly, with the increasing pH in soil during the remediation process and the existence of organic matter and other ions, a portion of the reduced Cr(III) would form some Cr(III) by-products such as $Cr(OH)_3$, Cr_2O_3, $CrCl_3$, as well as organic Cr(III) complexes. Meanwhile, the urease secreted by *S. saromensis* W5 hydrolyzed urea to produce CO_3^{2-}, while $CaCl_2$ was also decomposed to produce Ca^{2+}. Finally, the co-precipitation reaction of the reduced Cr(III) with CO_3^{2-} and Ca^{2+} would take place, and then the Cr(III) would be effectively stabilized in the form of $Ca_{10}Cr_6O_{24}(CO_3)$. Additionally, the pH value in soil would increase due to the urea hydrolysis, which could provide a stable microenvironment for forming the carbonate precipitation. In summary, microbially mediated reduction and co-precipitation with carbonate were the major mechanisms for immobilizing Cr(VI) from soil.

4 Conclusions

In this study, Cr(VI)-reducing bacterium induced carbonate precipitation was verified to be an effective restoration technique for Cr(VI)-contaminated soil. The increase of F3 form in BCR, the increase of soil urease activity and the decrease of Cr(VI) content, all of which indicated that W5 bacteria made a significant contribution in the MICP system. The restored soil had a higher organic matter content and the quality of contaminated soil was improved. Furthermore, a series of characterization analyses demonstrated that the main Cr stabilization mechanism in contaminated soil was the coprecipitation reaction for $CaCO_3$ and Cr. This study will provide an economical and environmentally friendly way to remediate Cr(VI)-contaminated soil, and further offer novel perspectives on the utilization of MICP technology in soil remediation.

Acknowledgements This work was financially supported by the National Natural Science Foundation of China (52270172), and the Key Research and Development International Cooperation Project (2022YFE0119600).

Author Contributions Chunyangzi Jiang: Data curation; Visualization; Formal analysis; Writing – original draft. Ni He: Writing – review & editing. Yayuan Liu: Writing – review & editing. Liang Hu: Conceptualization; Supervision; Funding acquisition; Writing – review & editing. Hongbo Zhao: Funding acquisition.

Data Availability Data will be made available on request.

Declarations

Competing Interests The authors declare no competing interests.

References

Altowayti, W. A. H., Algaifi, H. A., Bakar, S. A., & Shahir, S. (2019). The adsorptive removal of As (III) using biomass of arsenic resistant *Bacillus thuringiensis* strain WS3: Characteristics and modelling studies. *Ecotoxicology and Environmental Safety, 172*, 176–185. https://doi.org/10.1016/j.ecoenv.2019.01.067

Cai, Q., Xu, M., Ma, J., Zhang, X., Yang, G., Long, L., Chen, C., Wu, J., Song, C., & Xiao, Y. (2023). Improvement of cadmium immobilization in contaminated paddy soil by using ureolytic bacteria and rice straw. *Science of the Total Environment, 874*, 162594. https://doi.org/10.1016/j.scitotenv.2023.162594

Carter, H. T., Tipping, E., Koprivnjak, J.-F., Miller, M. P., Cookson, B., & Hamilton-Taylor, J. (2012). Freshwater DOM quantity and quality from a two-component model of UV absorbance. *Water Research, 46*(14), 4532–4542. https://doi.org/10.1016/j.watres.2012.05.021

Disi, Z. A., Attia, E., Ahmad, M. I., & Zouari, N. (2022). Immobilization of heavy metals by microbially induced

carbonate precipitation using hydrocarbon-degrading ureolytic bacteria. *Biotechnology Reports, 35*, e00747. https://doi.org/10.1016/j.btre.2022.e00747

Dong, H., Huang, L., Zhao, L., Zeng, Q., Liu, X., Sheng, Y., Shi, L., Wu, G., Jiang, H., Li, F., Zhang, L., Guo, D., Li, G., Hou, W., & Chen, H. (2022). A critical review of mineral-microbe interaction and co-evolution: mechanisms and applications. *National Science Review, 9*(10), nwac128. https://doi.org/10.1093/nsr/nwac128

Dou, X., Su, H., Xu, D., Liu, C., Meng, H., Li, H., Zhang, J., Dang, Y., Feng, L., Zhang, L., Du, Z., & Holmes, D. E. (2022). Enhancement effects of dissolved organic matter leached from sewage sludge on microbial reduction and immobilization of Cr(VI) by *Geobacter sulfurreducens*. *Science of the Total Environment, 835*, 155301. https://doi.org/10.1016/j.scitotenv.2022.155301

Fu, L., Feng, A., Xiao, J., Wu, Q., Ye, Q., & Peng, S. (2021). Remediation of soil contaminated with high levels of hexavalent chromium by combined chemical-microbial reduction and stabilization. *Journal of Hazardous Materials, 403*, 123847. https://doi.org/10.1016/j.jhazmat.2020.123847

Fu, T., Saracho, A. C., & Haigh, S. K. (2023). Microbially induced carbonate precipitation (MICP) for soil strengthening: A comprehensive review. *Biogeotechnics, 1*(1), 100002. https://doi.org/10.1016/j.bgtech.2023.100002

Gao, Y., Wang, H., Xu, R., Wang, Y.-n., Sun, Y., Bian, R., & Li, W. (2022). Remediation of Cr(VI)-contaminated soil by combined chemical reduction and microbial stabilization: The role of biogas solid residue (BSR). *Ecotoxicology and Environmental Safety*, *231*, Article 113198. https://doi.org/10.1016/j.ecoenv.2022.113198

He, Z. G., Li, S. Z., Wang, L. S., & Zhong, H. (2014). Characterization of five chromium-removing bacteria isolated from chromium-contaminated soil. *Water, Air, and Soil Pollution, 225*, 1904. https://doi.org/10.1007/s11270-014-1904-2

He, N., Hu, L., He, Z., Li, M., & Huang, Y. (2022a). Mineralization of lead by *Phanerochaete chrysosporium* microcapsules loaded with hydroxyapatite. *Journal of Hazardous Materials, 422*, 126902. https://doi.org/10.1016/j.jhazmat.2021.126902

He, N., Hu, L., Jiang, C., & Li, M. (2022b). Remediation of chromium, zinc, arsenic, lead and antimony contaminated acidic mine soil based on Phanerochaete chrysosporium induced phosphate precipitation. *Science of the Total Environment, 850*, 157995. https://doi.org/10.1016/j.scitotenv.2022.157995

He, N., Ran, M., Hu, L., Jiang, C., & Liu, Y. (2023). Periplasmic space is the key location for Pb(II) biomineralization by *Burkholderia cepacia*. *Journal of Hazardous Materials, 445*, 130465. https://doi.org/10.1016/j.jhazmat.2022.130465

Huang, Y., Zeng, Q., Hu, L., Xiong, D., Zhong, H., & He, Z. (2021a). Column study of enhanced Cr(VI) removal and removal mechanisms by *Sporosarcina saromensis* W5 assisted bio-permeable reactive barrier. *Journal of Hazardous Materials, 405*, 124115. https://doi.org/10.1016/j.jhazmat.2020.124115

Huang, Y., Zeng, Q., Hu, L., Zhong, H., & He, Z. (2021b). Bioreduction performances and mechanisms of Cr(VI) by *Sporosarcina saromensis* W5, a novel Cr(VI)-reducing facultative anaerobic bacteria. *Journal of Hazardous Materials, 413*, 125411. https://doi.org/10.1016/j.jhazmat.2021.125411

Jiang, C., Hu, L., He, N., Liu, Y., & Zhao, H. (2023). Bioreduction and mineralization of Cr(VI) by *Sporosarcina saromensis* W5 induced carbonate precipitation. *Environmental Science and Pollution Research International*. https://doi.org/10.1007/s11356-023-28536-3

Kumar, A., Song, H.-W., Mishra, S., Zhang, W., Zhang, Y.-L., Zhang, Q.-R., & Yu, Z.-G. (2023). Application of microbial-induced carbonate precipitation (MICP) techniques to remove heavy metal in the natural environment: A critical review. *Chemosphere, 318*, 137894. https://doi.org/10.1016/j.chemosphere.2023.137894

Li, F., Zheng, Y., Tian, J., Ge, F., Liu, X., Tang, Y., & Feng, C. (2019). Cupriavidus sp. strain Cd02-mediated pH increase favoring bioprecipitation of Cd2+ in medium and reduction of cadmium bioavailability in paddy soil. *Ecotoxicology and Environmental Safety, 184*, 109655. https://doi.org/10.1016/j.ecoenv.2019.109655

Li, W., Yang, Y., & Achal, V. (2022a). Biochemical composite material using corncob powder as a carrier material for ureolytic bacteria in soil cadmium immobilization. *Science of the Total Environment, 802*, 149802. https://doi.org/10.1016/j.scitotenv.2021.149802

Li, Y., Wen, J., Xue, Z., Yin, X., Yuan, L., & Yang, C. (2022b). Removal of Cr(VI) by polyaniline embedded polyvinyl alcohol/sodium alginate beads – Extension from water treatment to soil remediation. *Journal of Hazardous Materials, 426*, 127809. https://doi.org/10.1016/j.jhazmat.2021.127809

Li, L., Lv, Y., Jia, C., Yin, D., Dong, Z., Zhan, Z., Han, J., & Zhang, J. (2023). Preparation of sludge–cyanobacteria composite carbon for synergistically enhanced co-removal of Cu(II) and Cr(VI). *Chemosphere, 320*, 138043. https://doi.org/10.1016/j.chemosphere.2023.138043

Lin, X., Sun, Z., Zhao, L., Ma, J., Li, X., He, F., & Hou, H. (2019). Toxicity of exogenous hexavalent chromium to soil-dwelling springtail Folsomia candida in relation to soil properties and aging time. *Chemosphere, 224*, 734–742. https://doi.org/10.1016/j.chemosphere.2019.02.196

Liu, L., Sun, P., Chen, Y., Li, X., & Zheng, X. (2023). Distinct chromium removal mechanisms by iron-modified biochar under varying pH: Role of iron and chromium speciation. *Chemosphere, 331*, 138796. https://doi.org/10.1016/j.chemosphere.2023.138796

Long, B., Liao, L., Jia, F., Luo, Y., He, J., Zhang, W., & Shi, J. (2023). Oxalic acid enhances bioremediation of Cr(VI) contaminated soil using *Penicillium oxalicum* SL2. *Chemosphere, 311*, 136973. https://doi.org/10.1016/j.chemosphere.2022.136973

Luo, Y., Ye, B., Ye, J., Pang, J., Xu, Q., Shi, J., Long, B., & Shi, J. (2020). Ca^{2+} and SO42− accelerate the reduction of Cr(VI) by *Penicillium oxalicum* SL2. *Journal of Hazardous Materials, 382*, 121072. https://doi.org/10.1016/j.jhazmat.2019.121072

Luo, X., Zhou, X., Peng, C., Shao, P., Wei, F., Li, S., Liu, T., Yang, L., Ding, L., & Luo, X. (2022). Bioreduction performance of Cr(VI) by microbial extracellular polymeric substances (EPS) and the overlooked role of tryptophan. *Journal of Hazardous Materials, 433*, 128822. https://doi.org/10.1016/j.jhazmat.2022.128822

Ma, L., Du, Y., Chen, S., Du, D., Ye, H., & Zhang, T. C. (2022). Highly efficient removal of Cr(VI) from aqueous solution by pinecone biochar supported nanoscale zero-valent iron coupling with *Shewanella oneidensis* MR-1. *Chemosphere, 287*, 132184. https://doi.org/10.1016/j.chemosphere.2021.132184

Munir, M. A. M., Liu, G., Yousaf, B., Ali, M. U., Cheema, A. I., Rashid, M. S., & Rehman, A. (2020). Bamboo-biochar and hydrothermally treated-coal mediated geochemical speciation, transformation and uptake of Cd, Cr, and Pb in a polymetal(iod)s-contaminated mine soil. *Environmental Pollution, 265*(PT A), 114816. https://doi.org/10.1016/j.envpol.2020.114816

Nelson, D. W., & Sommers, L. E. (1982) Total carbon, organic carbon and organic matter: In A. L. Page, R. H. Miller, & D.R. Keeney (Eds.), *Methods of soil analysis. Part 2 Chemical and Microbiological Properties* (pp. 539–579).

Nie, M., Wu, C., Tang, Y., Shi, G., Wang, X., Hu, C., Cao, J., & Zhao, X. (2023). Selenium and *Bacillus proteolyticus* SES synergistically enhanced ryegrass to remediate Cu–Cd–Cr contaminated soil. *Environmental Pollution, 323*, 121272. https://doi.org/10.1016/j.envpol.2023.121272

Peng, D., Qiao, S., Luo, Y., Ma, H., Zhang, L., Hou, S., Wu, B., & Xu, H. (2020). Performance of microbial induced carbonate precipitation for immobilizing Cd in water and soil. *Journal of Hazardous Materials, 400*, 123116. https://doi.org/10.1016/j.jhazmat.2020.123116

Qian, X., Fang, C., Huang, M., & Achal, V. (2017). Characterization of fungal-mediated carbonate precipitation in the biomineralization of chromate and lead from an aqueous solution and soil. *Journal of Cleaner Production, 164*, 198–208. https://doi.org/10.1016/j.jclepro.2017.06.195

Sheng, M., Peng, D., Luo, S., Ni, T., Luo, H., Zhang, R., Wen, Y., & Xu, H. (2022). Micro-dynamic process of cadmium removal by microbial induced carbonate precipitation. *Environmental Pollution, 308*, 119585. https://doi.org/10.1016/j.envpol.2022.119585

Shi, J., McGill, W. B., Chen, N., Rutherford, P. M., Whitcombe, T. W., & Zhang, W. (2020). Formation and Immobilization of Cr(VI) Species in Long-Term Tannery Waste Contaminated Soils. *Environmental Science & Technology, 54*(12), 7226–7235. https://doi.org/10.1021/acs.est.0c00156

Song, M., Ju, T., Meng, Y., Han, S., Lin, L., & Jiang, J. (2022). A review on the applications of microbially induced calcium carbonate precipitation in solid waste treatment and soil remediation. *Chemosphere, 290*, 133229. https://doi.org/10.1016/j.chemosphere.2021.133229

Tang, J., Liu, Z., Liu, W., Finfrock, Y. Z., Ye, Z., Liu, X., & Liu, P. (2022). Application of Fe-doped biochar in Cr(VI) removal from washing wastewater and residual Cr(VI) immobilization in contaminated soil. *Journal of Cleaner Production, 380*, 134973. https://doi.org/10.1016/j.jclepro.2022.134973

Wani, K. I., Naeem, M., & Aftab, T. (2022). Chromium in plant-soil nexus: Speciation, uptake, transport and sustainable remediation techniques. *Environmental Pollution, 315*, 120350. https://doi.org/10.1016/j.envpol.2022.120350

Wei, T., Li, X., Li, H., Gao, H., Guo, J., Li, Y., Ren, X., Hua, L., & Jia, H. (2022). The potential effectiveness of mixed bacteria-loaded biochar/activated carbon to remediate Cd, Pb co-contaminated soil and improve the performance of pakchoi plants. *Journal of Hazardous Materials, 435*, 129006. https://doi.org/10.1016/j.jhazmat.2022.129006

Wen, J., Xue, Z., Yin, X., & Wang, X. (2022). Insights into aqueous reduction of Cr(VI) by biochar and its iron-modified counterpart in the presence of organic acids. *Chemosphere, 286*, 131918. https://doi.org/10.1016/j.chemosphere.2021.131918

Wu, M., Wang, Q., Wang, C., Zeng, Q., Li, J., Wu, H., Wu, B., Xu, H., & Qiu, Z. (2022a). Strategy for enhancing Cr(VI)-contaminated soil remediation and safe utilization by microbial-humic acid-vermiculite-alginate immobilized biocomposite. *Ecotoxicology and Environmental Safety, 243*, 113956. https://doi.org/10.1016/j.ecoenv.2022.113956

Wu, Q., Mo, W., Liu, J., Peng, S., Li, Q., & Wan, R. (2022b). Remediation of high-concentration Cr(VI)-contaminated soils with $FeSO_4$ combined with biostimulation: Cr(VI) transformation and stabilization. *Journal of Hazardous Materials Advances, 8*, 100161. https://doi.org/10.1016/j.hazadv.2022.100161

Xiao, W., Zhang, Q., Zhao, S., Chen, D., Gao, N., Huang, M., & Ye, X. (2023). Citric acid secretion from rice roots contributes to reduction and immobilization of Cr(VI) by driving microbial sulfur and iron cycle in paddy soil. *Science of the Total Environment, 854*, 158832. https://doi.org/10.1016/j.scitotenv.2022.158832

Xie, Y., Guan, Z., Cheng, J., Zhou, Y., & Yan, M. (2021). Competition between Al(III) and Fe(III) for binding onto natural organic matter: In situ monitoring by UV–Vis absorbance spectroscopy. *Chemosphere, 270*, 128655. https://doi.org/10.1016/j.chemosphere.2020.128655

Xie, L., Chen, Q., Liu, Y., Ma, Q., Zhang, J., Tang, C., Duan, G., Lin, A., Zhang, T., & Li, S. (2023). Enhanced remediation of Cr(VI)-contaminated soil by modified zero-valent iron with oxalic acid on biochar. *Science of the Total Environment, 905*, 167399. https://doi.org/10.1016/j.scitotenv.2023.167399

Xue, Z.-F., Cheng, W.-C., Wang, L., Qin, P., & Zhang, B. (2022). Revealing degradation and enhancement mechanisms affecting copper (Cu) immobilization using microbial-induced carbonate precipitation (MICP). *Journal of Environmental Chemical Engineering, 10*(5), 108479. https://doi.org/10.1016/j.jece.2022.108479

Zeng, Y., Chen, Z., Du, Y., Lyu, Q., Yang, Z., Liu, Y., & Yan, Z. (2021). Microbiologically induced calcite precipitation technology for mineralizing lead and cadmium in landfill leachate. *Journal of Environmental Management, 296*, 113199. https://doi.org/10.1016/j.jenvman.2021.113199

Zeng, Y., Chen, Z., Lyu, Q., Cheng, Y., Huan, C., Jiang, X., Yan, Z., & Tan, Z. (2023). Microbiologically induced calcite precipitation for in situ stabilization of heavy metals contributes to land application of sewage sludge. *Journal of Hazardous Materials, 441*, 129866. https://doi.org/10.1016/j.jhazmat.2022.129866

Zhang, H.-K., Lu, H., Wang, J., Zhou, J.-T., & Sui, M. (2014). Cr(VI) Reduction and Cr(III) Immobilization by *Acinetobacter sp* HK-1 with the Assistance of a Novel Quinone/Graphene Oxide Composite. *Environmental Science & Technology, 48*(21), 12876–12885. https://doi.org/10.1021/es5039084

Zhang, J., Su, P., & Li, L. (2022). Bioremediation of stainless steel pickling sludge through microbially induced

carbonate precipitation. *Chemosphere, 298*, 134213. https://doi.org/10.1016/j.chemosphere.2022.134213

Zhang, X., Li, Q., Nie, K., Cao, K., Liao, Q., Si, M., Yang, Z., & Yang, W. (2023). Synergistic effect of sulfidated nano zerovalent iron and proton-buffering montmorillonite in reductive immobilization of alkaline Cr(VI)-contaminated soil. *Chemosphere, 321*, 138132. https://doi.org/10.1016/j.chemosphere.2023.138132

Zhao, X., Tang, D., & Jiang, Y. (2021). Effect of the reduction-mineralization synergistic mechanism of *Bacillus* on the remediation of hexavalent chromium. *Science of the Total Environment, 777*, 146190. https://doi.org/10.1016/j.scitotenv.2021.146190

Zheng, T., & Qian, C. (2020). Influencing factors and formation mechanism of $CaCO_3$ precipitation induced by microbial carbonic anhydrase. *Process Biochemistry, 91*, 271–281. https://doi.org/10.1016/j.procbio.2019.12.018

Zou, D., Tong, J., Feng, C., Wang, Y., Li, X., Zheng, X., Wang, X., & Liu, Y. (2022). Synthesis of biochar@α-Fe_2O_3@*Shewanella loihica* complex for remediation of soil contaminated by hexavalent chromium: Optimization of conditions and mechanism. *Chemosphere, 303*, 134858. https://doi.org/10.1016/j.chemosphere.2022.134858